Observation of Excitonic Rydberg States in Monolayer MoS$_2$ and WS$_2$ by Photoluminescence Excitation Spectroscopy

Heather M. Hill,[†] Albert F. Rigosi,[†] Cyrielle Roquelet,[†] Alexey Chernikov,[†] Timothy C. Berkelbach,[‡] David R. Reichman,[‡] Mark S. Hybertsen,[§] Louis E. Brus,[‡] and Tony F. Heinz*,[†,‖]

[†]Departments of Physics and Electrical Engineering and [‡]Department of Chemistry, Columbia University, New York, New York 10027, United States

[§]Center for Functional Nanomaterials, Brookhaven National Laboratory, Upton, New York 11973, United States

Ⓢ *Supporting Information*

ABSTRACT: We have identified excited exciton states in monolayers of MoS$_2$ and WS$_2$ supported on fused silica by means of photoluminescence excitation spectroscopy. In monolayer WS$_2$, the positions of the excited A exciton states imply an exciton binding energy of 0.32 eV. In monolayer MoS$_2$, excited exciton transitions are observed at energies of 2.24 and 2.34 eV. Assigning these states to the B exciton Rydberg series yields an exciton binding energy of 0.44 eV.

KEYWORDS: *Transition metal dichalcogenides, molybdenum disulfide, tungsten disulfide, 2D materials, binding energy, excitons*
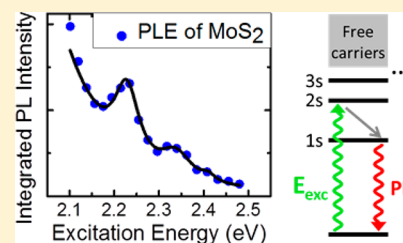
Atomically thin crystals of transition metal dichalcogenides (TMDCs) in the family of MoS$_2$, MoSe$_2$, WS$_2$, and WSe$_2$ have attracted much recent attention because of their distinctive physical properties, including an indirect-to-direct band gap transition in the monolayer limit,[1−4] efficient luminescence and light-matter interactions,[1−11] and strong coupling of the valley and spin degrees of freedom.[12−21] The materials have also shown potential for use in various optoelectronic devices,[22−24] and the growth of high-quality, large-area crystals has been reported in several studies.[25−31] One of the most intriguing properties arising from the reduced dimensionality of these materials is the strong enhancement of Coulomb interactions that they exhibit. This leads to pronounced many-body effects, such as charged excitons with binding energies in the range of 30 meV.[32,33]

Much effort has been focused on the excitonic properties of these materials, particularly on the exciton binding energies and the spectrum of excited excitonic states. Despite much theoretical progress,[34−45] direct experimental information on this topic has only begun to appear.[46−50] In particular, for the important case of the MoS$_2$ monolayer the values for the exciton binding energy have remained elusive. Recently, reports using scanning tunneling spectroscopy[51] (STS) and photocurrent[52] measurements infer the quasi-particle band gap in monolayer MoS$_2$. Our study uses purely optical measurements to identify directly transitions in the exciton Rydberg series. These states have yet to be observed in MoS$_2$ monolayers and provide an alternative approach to the study of excitonic interactions and binding energy. In such purely optical studies, the primary obstacle lies in the difficulty of observing excited exciton states or the signature of transitions to the continuum states. These transitions are concealed not only by their relative

weakness but also by their increased spectral width compared with the ground-state exciton. These difficulties are compounded by the presence of absorption from the tail of higher-lying resonances, such as the so-called C transition attributed to the interband transitions around the Γ-point of the Brillouin zone.[41,53]

In this work, we address this issue by using one-photon photoluminescence excitation (PLE) spectroscopy, taking advantage of differences in the relative contributions of the excitonic states and the background to the photoluminescence quantum efficiency (QE). More specifically, we report the observation of excited (Rydberg) exciton states in monolayer MoS$_2$ and WS$_2$ at room temperature. From the peak positions, we infer a binding energy of 0.32 ($\pm$0.05) eV for the A exciton in WS$_2$, which is in agreement with our previous low-temperature study by reflectance spectroscopy.[47] In the PLE spectra of MoS$_2$ monolayers, excited exciton states are observed at average energies of 2.24 ($\pm$0.02) eV and 2.34 ($\pm$0.03) eV. If we assign these transitions to the Rydberg series of the A exciton, we infer an exciton binding energy of 0.64 ($\pm$0.08) eV. An alternative assignment associates them with excited states of the B exciton, implying a binding energy for the corresponding exciton of 0.44 ($\pm$0.08) eV. Comparison with the results for WS$_2$ and theoretical considerations favor the latter interpretation but the former cannot be fully excluded.

The experiments were conducted on mechanically exfoliated monolayers of MoS$_2$ and WS$_2$ prepared on fused silica substrates. Additional measurements were taken on monolayer
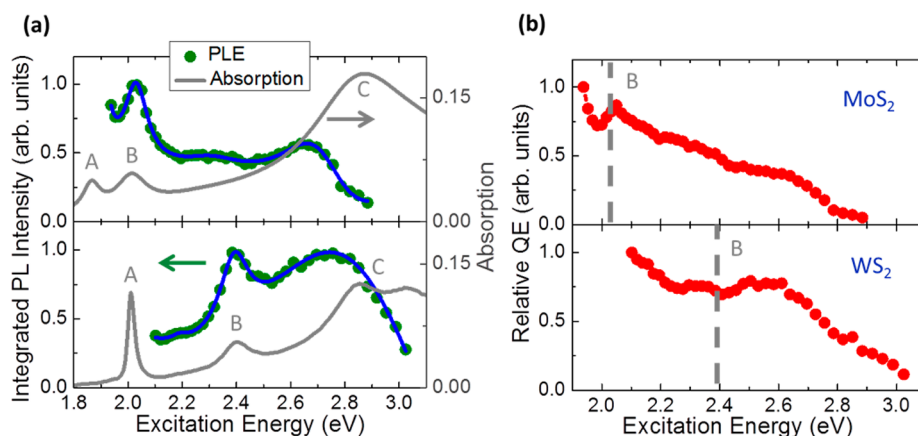
Figure 1. (a). PLE (left axis) and absorption (right axis) spectra for monolayer MoS_2 (top) and WS_2 (bottom) monolayers, both on fused silica substrates. The PLE spectra are normalized to the intensity at the B peak. The smooth blue curve is a guide to the eye. (b) The relative quantum efficiency (QE) of MoS_2 and WS_2 monolayers in arbitrary units normalized to the highest value in range.

MoS_2 on a flake of crystalline h-BN of about 20 nm thickness supported on a silicon substrate with a 300 nm oxide epilayer. Samples on h-BN exhibited significantly higher PL efficiency, which enhanced the observation of the PLE features. The layer thickness of MoS_2 and WS_2 samples was confirmed by PL and Raman spectroscopy. The PLE measurements were performed under ambient conditions using a pulsed supercontinuum laser source, filtered by a grating monochromator to provide tunable excitation of 1.5 nm bandwidth. The laser operated at a 40 MHz repetition rate with a pulse duration of approximately 400 fs. The sample was excited with a beam having an average power of 100 nW and a spot size of 2-μm radius. The typical exciton density created in the monolayer by each excitation pulse was $\sim 2 \times 10^9$ cm^{-2}, which lies below the range for which significant exciton−exciton annihilation is expected[54] (see Supporting Information). For each excitation wavelength, a PL (emission) spectrum was recorded and integrated over the A peak emission to obtain the corresponding value in the PLE spectrum (see Supporting Information). The relative QE is obtained from the PLE spectra by normalizing for the absorption and variation in excitation photon energy. The absorption spectra were obtained from reflectance contrast measurements[55] performed with a tungsten−halogen source and an inverted microscope paired with a grating spectrometer and a liquid-nitrogen cooled charge-coupled device detector.

Figure 1a shows the PLE and absorption spectra for monolayer MoS_2 and WS_2 crystals on fused silica substrates. (See Supporting Information for the power, sample, and substrate dependence of the PLE spectra.) For both materials, the PLE spectrum increases, as expected, at the energy of the B exciton. At higher photon energies, the absorption increases as we approach the strong C transition, which is attributed to higher-lying transitions away from the K/K′ point of the Brillouin zone.[41,53] The PLE signal, however, remains flat or decreases with increasing photon energy. The general shape of our PLE spectra agrees well with those recently reported in a study of TMDC monolayers by Kozawa et al.[56]

The corresponding relative QE is presented in Figure 1b for the two samples. (See the Supporting Information for the QE of the MoS_2 on h-BN substrate sample.) In both cases, the relative QE decreases significantly with increasing photon energy. The QE falls by nearly a factor of 10 around the C resonance compared to excitation of B exciton and the high-

energy side of the A exciton, as previously observed by Kozawa et al.[56]

In an ideal system with fast relaxation of the electron−hole pairs toward the lowest energy excitonic state, negligible nonradiative recombination, and no multiple carrier generation, one would expect the QE to be near unity and independent of the excitation energy. The PLE spectrum would then simply match the optical absorption spectrum. However, for the studied materials the data indicates the existence of competition between the relaxation processes to the A exciton (and subsequent emission) and efficient nonradiative decay channels, the latter having a dependence on the excess carrier energy. In the study by Kozawa et al.,[56] the authors examined the relaxation pathways for carriers excited by higher-energy visible photons. They concluded that the majority of these carriers are excited in band nesting regions of the Brillouin zone[41,53] near the Γ point with dominant relaxation pathways toward the Λ point for electrons and toward the Γ point for holes. The impeded relaxation of these carriers to the K/K′ valleys in the presence of rapid nonradiative recombination processes thus leads to a decrease in the QE. The excited states of the A and B excitons, however, correspond to transitions at the K/K′ points and are expected to exhibit efficient relaxation toward the lowest energy exciton state, as has been observed in GaAs quantum wells.[57] The reduced QE for excitation of the wing of the C peak thus suppresses the spectral background present around the excited excitonic states, making the latter states more readily discernible in the PLE spectrum than in direct absorption measurements.

We now turn to the study of excited states of the excitons or exciton Rydberg series revealed in the PLE measurements. The levels are denoted as 1s (for the lowest-energy exciton state), and as 2s, 3s, 4s,... for the optically accessible excited excitonic states. For the WS_2 monolayer on fused silica, we observe a series of peaks in the room-temperature PLE spectrum at energies between the A and B excitons (Figure 2). After allowing for a temperature-dependent spectral shift associated with the change in the band gap, these features match those observed in the low-temperature absorption measurements in our previous study and can be identified as members of the Rydberg series of the A exciton.[47] In Figure 2, we compare the PLE spectrum with the reflectance contrast spectrum, after differentiating the latter with respect to energy to bring out the spectral features more clearly. We find good agreement
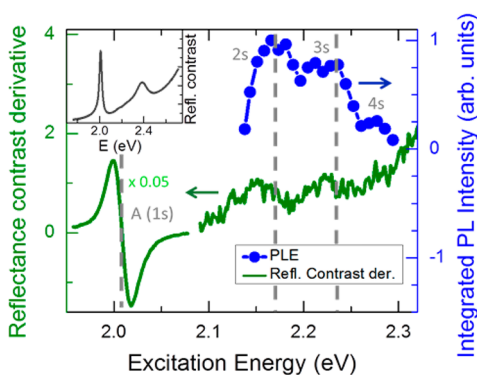
Figure 2. Spectroscopy of excitonic states in monolayer WS_2. The normalized PLE spectrum (right axis) after subtraction of a smooth background (as described in the Supporting Information) and the derivative of the reflectance contrast spectrum (left axis) of monolayer WS_2 on a fused silica substrate. The A exciton 1s peak is divided by a factor of 20. The positions of the A exciton 1s, 2s, and 3s states are marked by dashed lines. The inset shows the original reflectance contrast spectrum over a wider spectral range, where the two strong features correspond to the 1s transitions of the A and B excitons.

Figure 3. PLE spectroscopy results for excited excitonic states in monolayer MoS_2. (a) The PLE spectra of monolayer MoS_2 samples supported on fused silica substrates and on a thick h-BN flake on a Si/SiO_2 substrate. The smooth black curves are guides to the eye. The spectra have been normalized to their peak intensity and offset for clarity. The dashed lines indicate the 2s and 3s exciton states. (b) Experimental energies for the 1s, 2s, and 3s exciton states in monolayer MoS_2 from PLE measurements (dots) and theoretical values for the corresponding transitions obtained using the nonlocal screening model described in the text. The calculated band gap is marked by a dashed line.

between the peak positions determined by these two spectroscopic approaches.

As shown in our previous study[47] and in other investigations of monolayer TMDCs,[46,49] the energies of the excited excitonic states deviate strongly from a simple 2D hydrogenic model due to the nonuniform dielectric environment. Because the electric field between the electron and hole is not confined in the plane of the material but also extends into the surrounding medium, the effective screening of the Coulomb interaction depends on the separation between the charges. However, for the large electron−hole separations characteristic of the higher-lying states (with $n \geq 3$), the hydrogenic model was found to provide a reasonable approximation of the energy-level structure.[47]

We can therefore determine the quasiparticle band gap as the continuum limit of a hydrogenic spectrum, which we fit to the measured transition energies of the 3s and 4s bound states for the WS_2 monolayer. This procedure yields a band gap of 2.33 (± 0.05) eV and an exciton binding energy of 0.32 (± 0.05) eV, which is in agreement with the previous low-temperature result.[47] This further confirms our assignment of the PLE features to the excited states of the exciton.

The PLE spectrum of monolayer MoS_2, presented in Figure 3a, is given for a sample on fused silica and a sample on a h-BN flake on a Si/SiO_2 substrate. The sample on BN exhibits higher PL intensity, which allows the weaker features in the PLE spectrum to be identified more clearly. The energies of the additional features in the PLE spectra differ very slightly (~10 meV) in the two samples, possibly due to the different dielectric environment from the different substrates. In following discussion we use an averaged value for the excited state energies.

The PLE spectrum of MoS_2 is generally similar to that measured for WS_2 with two clearly discernible excited-state transitions. However, in the case of MoS_2 an additional complication arises in terms of the assignment of the peaks: we need to consider whether the observed peaks form part of the A or B exciton Rydberg series, because the 0.15 eV splitting between A and B peak is not large enough to make the analysis obvious as in the case of WS_2. Below we consider the different possible peak assignments.

One possible assignment would be to associate the two observed features with the lowest-lying (2s) excited states of the A and B exciton series. However, we are able to exclude this interpretation based on the following reasoning. The observed transition energies of 2.24 (± 0.02) and 2.34 (± 0.03) eV for the two features differ by only 0.10 eV, while the splitting between the A and B excitons is 0.15 eV (see the absorption spectra in Figure 1a). If we assume the binding energy is the same for the A and B exciton, we would expect the excited features observed to have the same energy spacing as the 1s peaks. The calculated reduced mass for the B exciton mass is slightly higher than that of the A exciton.[43,44] Assuming the mass scaling of the hydrogenic model with reduced exciton masses[38] of $0.28m_0$ and $0.25m_0$ for the B and A exciton, respectively, we would expect the spacing between the 2s states of the A and B excitons to be 0.19 eV. This further enhances the discrepancy with experiment where the energy difference between the two states is only 0.10 eV. We note moreover that the higher-energy peak has only about half of the oscillator strength of the lower-energy peak. This cannot be understood in terms of an assignment as the states of the A and B exciton but is expected if the two features correspond to the 2s and 3s transitions in a Rydberg series, as in the two alternative assignments.

We still have, however, the ambiguity of whether these are the 2s and 3s states of the A or of the B exciton. In the former case, we infer a binding energy of 0.64 (± 0.08) eV (see Supporting Information). While this is a possible assignment, it poses two issues. First, the binding energy is about twice that of WS_2. On the basis of the theoretically calculated binding energies[37,38,42] there is no justification for such a large difference. Second, if the observed features form part of the A exciton Rydberg series, then we would expect to observe the excited states of the B exciton as well. No additional features are, however, seen in the PLE spectra.

Our preferred interpretation is, therefore, that we are observing peaks in the Rydberg series of the B exciton. The oscillator strengths inferred from the PLE spectra are compatible with this interpretation and provide further

evidence against the assignment of 2s transitions to the A and B exciton. To analyze the oscillator strengths, we fit the PLE features to Lorentzian lineshapes and compute the area. We find that relative to the 1s feature of the B exciton the oscillator strength for the 2s and 3s peaks are 0.22 ($\pm$0.07) and 0.10 ($\pm$0.08), respectively. This behavior is similar to that seen above for the Rydberg series in WS_2, where the A exciton 2s and 3s peaks had, respectively, relative oscillator strengths of 0.14 ($\pm$0.06) and 0.06 ($\pm$0.03). Assigning the MoS_2 PLE peaks to the Rydberg series of the B exciton and assuming that the A and B excitons have similar properties, we would expect to see the 2s and 3s transitions of the A exciton around 2.05 and 2.15 eV. The absence of such features in our PLE spectra can be readily understood by their overlap with the strong 1s transition of the B exciton. Thus, the picture for the interpretation of the features as the Rydberg series of the B exciton is compatible with all experimental observations.

To extract the quasi-particle band gap from the energies of the 1s, 2s, and 3s excitonic states we must use a theoretical treatment beyond that of the 2D hydrogenic model, because this approximation is not valid for these lowest-lying excitonic states.[46,47,49] We turn, consequently, to a more realistic theory of the energy-level structure of the excitonic states in transition metal dichalcogenides, which is based on a modified Coulomb interaction reflecting the nonlocal character of the dielectric screening.[38,47] This theoretical analysis yields a band gap of 2.47 eV, implying that the binding energy of the B exciton in MoS_2 is 0.44 ($\pm$0.08) eV. Compared to the A exciton in WS_2, the slightly larger binding energy of the B exciton in MoS_2 can be attributed to the higher effective mass of the excitons in MoS_2 compared to WS_2. The B exciton energies of MoS_2, summarized in Figure 3b, exhibit similar deviation from the 2D hydrogenic series as in WS_2 monolayers. The theoretical model captures the experimentally observed behavior. In this calculation an exciton reduced mass of $\mu = 0.28m_0$ and a 2D polarizability of $\chi_{2D} = 9.3$ Å were used. The value of the reduced mass is taken from calculations in ref 38; the band gap and 2D polarizability are adjustable parameters. As in our previous work, we found it necessary to use a larger 2D polarizability than is calculated for intrinsic MoS_2 to account for doping and substrate effects. The binding energy of excitons in undoped, suspended MoS_2 monolayers should be, accordingly, somewhat larger than the value reported here.

Two recent experiments have inferred the exciton binding energy in monolayer MoS_2 using methods to determine the quasi-particle gap, which could then be compared with the measured 1s exciton transition energy. Zhang et al.[51] used scanning tunneling spectroscopy (STS) of MoS_2 monolayers on a graphite substrate. They observed two possible thresholds in the STS spectra and accordingly quote two possible exciton binding energies, 0.22 ($\pm$0.1) eV or 0.42 ($\pm$0.1) eV. The second value agrees within uncertainty with our B exciton assignment of 0.44 eV, supporting this assignment. Also, the dielectric screening from the graphite substrate could account for slight discrepancies between our results. Klots et al.[52] inferred a quasi-particle gap from photocurrent measurements of a suspended MoS_2 monolayer. They deduced an exciton binding energy $\geq$0.57 eV. Although substantially greater than the preferred exciton binding energy of 0.44 eV deduced in this work, the higher value inferred from the photocurrent measurements may reflect the reduced dielectric screening for the suspended sample.

In conclusion, we have introduced one-photon PLE spectroscopy as a convenient method to study excited states of excitons in TMDCs. The PLE spectra show clear features of the exciton Rydberg series of WS_2 and MoS_2 monolayers, yielding exciton binding energies of 0.32 ($\pm$0.05) eV for the WS_2 A exciton, which is in agreement with our earlier study[47] based on reflectance spectroscopy. For the case of the MoS_2 monolayer, we report the first observation of the excited exciton states. We infer an exciton binding energy of 0.44 ($\pm$0.08) eV, consistent with other recent experimental analyses, based on the assignment of our spectra to excited states of the B exciton. A less likely assignment of the excited states to the A exciton yields a binding energy of 0.64 ($\pm$0.08) eV.

■ ASSOCIATED CONTENT

Ⓢ Supporting Information

Photoluminescence excitation measurements, PL spectrum of sample, WS_2 PLE spectrum including the background contribution, exciton binding energy of MoS_2 for the alternative spectroscopic assignment of the PLE features, fits of PLE spectrum for MoS_2, and analysis of relative oscillator strengths. This material is available free of charge via the Internet at http://pubs.acs.org.

■ AUTHOR INFORMATION

Corresponding Author
*E-mail: tony.heinz@columbia.edu.

Present Address
∥Department of Applied Physics, Stanford University, Stanford, CA, 94305, United States and SLAC National Accelerator Laboratory, 2575 Sand Hill Road, Menlo Park, CA 94025, United States.

Author Contributions
The manuscript was written through contributions of all authors. All authors have given approval to the final version of the manuscript.

Notes
The authors declare no competing financial interest.

■ ACKNOWLEDGMENTS

Columbia University through Grant DE-AC05-06OR23100 (T.C.B.).

■ ABBREVIATIONS

TMDC, transition metal dichalcogenide; PL, photoluminescence; PLE, photoluminescence excitation; QE, quantum efficiency

■ REFERENCES

(1) Mak, K. F.; Lee, C.; Hone, J.; Shan, J.; Heinz, T. F. *Phys. Rev. Lett.* **2010**, *105*, 136805.

(2) Splendiani, A.; Sun, L.; Zhang, Y.; Li, T.; Kim, J.; Chim, C.; Galli, G.; Wang, F. *Nano Lett.* **2010**, *10*, 1271−5.

(3) Zhao, W.; Ghorannevis, Z.; Chu, L.; Toh, M.; Kloc, C.; Tan, P.; Eda, G. *ACS Nano* **2013**, *7*, 791−797.

(4) Ruppert, C.; Aslan, O. B.; Heinz, T. F. *Nano Lett.* **2014**, *14* (11), 6231−6236.

(5) Eda, G.; Yamaguchi, H.; Voiry, D.; Fujita, T.; Chen, M.; Chhowalla, M. *Nano Lett.* **2011**, *11*, 5111−5116.

(6) Bernardi, M.; Palummo, M.; Grossman, J. C. *Nano Lett.* **2013**, *13*, 3664−3670.

(7) Britnell, L.; Ribeiro, R. M.; Eckmann, A.; Jalil, R.; Belle, B. D.; Mishchenko, A.; Kim, Y.-J.; Gorbachev, R. V.; Georgiou, T.; Morozov, S. V.; Grigorenko, A. N.; Geim, A. K.; Casiraghi, C.; Castro Neto, A. H.; Novoselov, K. S. *Science* **2013**, *340*, 1311−4.

(8) Shen, C.-C.; Hsu, Y.-T.; Li, L.-J.; Liu, H.-L. *Appl. Phys. Express* **2013**, *6*, 125801.

(9) Li, Y.; Chernikov, A.; Zhang, X.; Rigosi, A.; Hill, H. M.; van der Zande, A. M.; Chenet, D. A.; Shih, E.-M.; Hone, J.; Heinz, T. F. *Phys. Rev. B* **2014**, *90*, 205422.

(10) Scheuschner, N.; Ochedowski, O.; Kaulitz, A.-M.; Gillen, R.; Schleberger, M.; Maultzsch, J. *Phys. Rev. B* **2014**, *89*, 125406.

(11) Yim, C.; O'Brien, M.; McEvoy, N.; Winters, S.; Mirza, I.; Lunney, J. G.; Duesberg, G. S. *Appl. Phys. Lett.* **2014**, *104*, 103114.

(12) Cao, T.; Wang, G.; Han, W.; Ye, H.; Zhu, C.; Shi, J.; Niu, Q.; Tan, P.; Wang, E.; Liu, B.; Feng, J. *Nat. Commun.* **2012**, *3*, 887.

(13) Mak, K. F.; He, K.; Shan, J.; Heinz, T. F. *Nat. Nanotechnol.* **2012**, *7*, 494−498.

(14) Sallen, G.; Bouet, L.; Marie, X.; Wang, G.; Zhu, C. R.; Han, W. P.; Lu, Y.; Tan, P. H.; Amand, T.; Liu, B. L.; Urbaszek, B. *Phys. Rev. B* **2012**, *86*, 081301.

(15) Zeng, H.; Dai, J.; Yao, W.; Xiao, D.; Cui, X. *Nat. Nanotechnol.* **2012**, *7*, 490−3.

(16) Xiao, D.; Liu, G.-B.; Feng, W.; Xu, X.; Yao, W. *Phys. Rev. Lett.* **2012**, *108*, 196802.

(17) Jones, A. M.; Yu, H.; Ghimire, N. J.; Wu, S.; Aivazian, G.; Ross, J. S.; Zhao, B.; Yan, J.; Mandrus, D. G.; Yao, W.; Xiao, D.; Xu, X. *Nat. Nanotechnol.* **2013**, *8*, 634−638.

(18) Lagarde, D.; Bouet, L.; Marie, X.; Zhu, C. R.; Liu, B. L.; Amand, T.; Tan, P. H.; Urbaszek, B. *Phys. Rev. Lett.* **2014**, *112*, 047401.

(19) Mak, K. F.; McGill, K. L.; Park, J.; McEuen, P. L. *Science* **2014**, *344*, 1489−1492.

(20) Wang, G.; Bouet, L.; Lagarde, D.; Vidal, M.; Balocchi, A.; Amand, T.; Marie, X.; Urbaszek, B. *Phys. Rev. B* **2014**, *90*, 075413.

(21) Xu, X.; Yao, W.; Xiao, D.; Heinz, T. F. *Nat. Phys.* **2014**, *10*, 343−350.

(22) Wang, Q. H.; Kalantar-Zadeh, K.; Kis, A.; Coleman, J. N.; Strano, M. S. *Nat. Nanotechnol.* **2012**, *7*, 699−712.

(23) Butler, S. Z.; Hollen, S. M.; Cao, L.; Cui, Y.; Gupta, J. A.; Gutiérrez, H. R.; Heinz, T. F.; Hong, S. S.; Huang, J.; Ismach, A. F.; Johnston-Halperin, E.; Kuno, M.; Plashnitsa, V. V.; Robinson, R. D.; Ruoff, R. S.; Salahuddin, S.; Shan, J.; Shi, L.; Spencer, M. G.; Terrones, M.; Windl, W.; Goldberger, J. E. *ACS Nano* **2013**, *7* (4), 2898−2926.

(24) Jariwala, D.; Sangwan, V. K.; Lauhon, L. J.; Marks, T. J.; Hersam, M. C. *ACS Nano* **2014**, *8* (2), 1102−1120.

(25) Lee, Y.-H.; Zhang, X.-Q.; Zhang, W.; Chang, M.-T.; Lin, C.-T.; Chang, K.-D.; Yu, Y.-C.; Wang, J. T.-W.; Chang, C.-S.; Li, L.-J.; Lin, T.-W. *Adv. Mater.* **2012**, *24* (17), 2320−2325.

(26) Gutiérrez, H. R.; Perea-López, N.; Elías, A. L.; Berkdemir, A.; Wang, B.; Lv, R.; López-Urías, F.; Crespi, V. H.; Terrones, H.; Terrones, M. *Nano Lett.* **2013**, *13* (8), 3447−3454.

(27) Lee, Y.-H.; Yu, L.; Wang, H.; Fang, W.; Ling, X.; Shi, Y.; Lin, C.-T.; Huang, J.-K.; Chang, M.-T.; Chang, C.-S.; Dresselhaus, M.; Palacios, T.; Li, L.-J.; Kong, J. *Nano Lett.* **2013**, *13* (4), 1852−1857.

(28) Najmaei, S.; Liu, Z.; Zhou, W.; Zou, X.; Shi, G.; Lei, S.; Yakobson, B. I.; Idrobo, J.-C.; Ajayan, P. M.; Lou, J. *Nat. Mater.* **2013**, *12*, 754−759.

(29) van der Zande, A. M.; Huang, P. Y.; Chenet, D. A.; Berkelbach, T. C.; You, Y.; Lee, G.-H.; Heinz, T. F.; Reichman, D. R.; Muller, D. A.; Hone, J. C. *Nat. Mater.* **2013**, *12*, 554−561.

(30) Gong, Y.; Lin, J.; Wang, X.; Shi, G.; Lei, S.; Lin, Z.; Zou, X.; Ye, G.; Vajtai, R.; Yakobson, B. I.; Terrones, H.; Terrones, M.; Tay, B. K.; Lou, J.; Pantelides, S. T.; Liu, Z.; Zhou, W.; Ajayan, P. M. *Nat. Mater.* **2014**, *13*, 1135−1142.

(31) Wang, X.; Gong, Y.; Shi, G.; Chow, W. L.; Keyshar, K.; Ye, G.; Yajtai, R.; Lou, J.; Liu, Z.; Ringe, E.; Tay, B. K.; Ajayan, P. M. *ACS Nano* **2014**, *8* (5), 5125−5131.

(32) Mak, K. F.; He, K.; Lee, C.; Lee, G. H.; Hone, J.; Heinz, T. F.; Shan, J. *Nat. Mater.* **2013**, *12*, 207−211.

(33) Ross, J. S.; Wu, S.; Yu, H.; Ghimire, N. J.; Jones, A. M.; Aivazian, G.; Yan, J.; Mandrus, D. G.; Xiao, D.; Yao, W.; Xu, X. *Nat. Commun.* **2013**, *4*, 1474.

(34) Cheiwchanchamnangij, T.; Lambrecht, W. R. L. *Phys. Rev. B* **2012**, *85*, 205302.

(35) Feng, J.; Qian, X.; Huang, C.-W.; Li, J. *Nat. Photonics* **2012**, *6*, 866−872.

(36) Komsa, H.-P.; Krasheninnikov, A. V. *Phys. Rev. B* **2012**, *86*, 241201.

(37) Ramasubramaniam, A. *Phys. Rev. B* **2012**, *86*, 115409.

(38) Berkelbach, T. C.; Hybertsen, M. S.; Reichman, D. R. *Phys. Rev. B* **2013**, *88*, 045318.

(39) Hüser, F.; Olsen, T.; Thygesen, K. S. *Phys. Rev. B* **2013**, *88*, 245309.

(40) Molina-Sánchez, A.; Sangalli, D.; Hummer, K.; Marini, A.; Wirtz, L. *Phys. Rev. B* **2013**, *88*, 045412.

(41) Qiu, D. Y.; da Jornada, F. H.; Louie, S. G. *Phys. Rev. Lett.* **2013**, *111*, 216805.

(42) Shi, H.; Pan, H.; Zhang, Y.-W.; Yakobson, B. I. *Phys. Rev. B* **2013**, *87*, 155304.

(43) Berghäuser, G.; Malic, E. *Phys. Rev. B* **2014**, *89*, 125309.

(44) Steinhoff, A.; Rösner, M.; Jahnke, F.; Wehling, T. O.; Gies, C. *Nano Lett.* **2014**, *14* (7), 3743−3748.

(45) Wu, F.; Qu, F.; MacDonald, A. H. *Phys. Rev. B* **2015**, *91*, 075310.

(46) He, K.; Kumar, N.; Zhao, L.; Wang, Z.; Mak, K. F.; Zhao, H.; Shan, J. *Phys. Rev. Lett.* **2014**, *113*, 026803.

(47) Chernikov, A.; Berkelbach, T. C.; Hill, H. M.; Rigosi, A.; Li, Y.; Aslan, O. B.; Reichman, D. R.; Hybertsen, M. S.; Heinz, T. F. *Phys. Rev. Lett.* **2014**, *113*, 076802.

(48) Ugeda, M. M.; Bradley, A. J.; Shi, S.-F.; da Jornada, F. H.; Zhang, Y.; Qiu, D. Y.; Ruan, W.; Mo, S.-K.; Hussain, Z.; Shen, Z.-S.; Wang, F.; Louie, S. G.; Crommie, M. F. *Nat. Mater.* **2014**, *13*, 1091−1095.

(49) Ye, Z.; Cao, T.; O'Brien, K.; Zhu, H.; Yin, X.; Wang, Y.; Louie, S. G.; Zhang, X. *Nature* **2014**, *513*, 214−218.

(50) Wang, G.; Marie, X.; Gerber, I.; Amand, T.; Lagarde, D.; Bouet, L.; Vidal, M.; Balocchi, A.; Urbaszek, B. **2016**, arXiv:1404.0056 [cond-mat.mtrl-sci]; accessed Oct 3, 2014.

(51) Zhang, C.; Johnson, A.; Hsu, C.-L.; Li, L.-J.; Shih, C.-K. *Nano Lett.* **2014**, *14* (5), 2443−7.

(52) Klots, A. R.; Newaz, A. K. M.; Wang, B.; Prasai, D.; Krzyzanowska, H.; Lin, J.; Caudel, D.; Ghimire, N. J.; Yan, J.; Ivanov, B. L.; Velizhanin, K. A.; Burger, A.; Mandrus, D. G.; Tolk, N. H.; Pantelides, S. T.; Bolotin, K. I. *Sci. Rep.* **2014**, *4*, 6608.

(53) Carvalho, A.; Ribeiro, R. M.; Castro Neto, A. H. *Phys. Rev. B* **2013**, *88*, 115205.

(54) Sun, D.; Rao, Y.; Reider, G. A.; Chen, G.; You, Y.; Brézin, L.; Harutyunyan, A. R.; Heinz, T. F. *Nano Lett.* **2014**, *14* (10), 5625−5629.

(55) Mak, K. F.; Sfeir, M. Y.; Wu, Y.; Lui, C. H.; Misewich, J. A.; Heinz, T. F. *Phys. Rev. Lett.* **2008**, *101*, 196405.

(56) Kozawa, D.; Kumar, R.; Carvalho, A.; Kumar, A. K.; Zhao, W.; Wang, S.; Toh, M.; Ribeiro, R. M.; Castro Neto, A. H.; Matsuda, K.; Eda, G. *Nat. Commun.* **2014**, *5*, 4543.

(57) Huber, R.; Schmid, B. A.; Kaindl, R. A.; Chemla, D. S. *Phys. Status Solidi B* **2008**, *6*, 1041−1048.